Advances in Nano Research, *Vol. 14, No. 4 (2023) 375-389*
https://doi.org/10.12989/anr.2023.14.4.375

The finite element method for dynamics of FG porous truncated conical panels reinforced with graphene platelets based on the 3-D elasticity

Lingqin Xia*[1,2], Ruiquan Wang[1], Guang Chen[1], Kamran Asemi**[3] and Abdelouahed Tounsi***[4,5,6]

[1]*Department of Additive Manufacturing, Zhejiang Institute of Mechanical & Electrical Engineering, hangzhou,310053, China*
[2]*Zhejiang Huashuo Technology Co.,Ltd., Ningbo, 315825, China*
[3]*Department of Mechanical Engineering, Islamic Azad University, North Tehran Branch, Tehran, Iran*
[4]*YFL (Yonsei Frontier Lab), Yonsei University, Seoul, Korea*
[5]*Material and Hydrology Laboratory, University of Sidi Bel Abbes, Faculty of Technology, Civil Engineering Department, Algeria*
[6]*Department of Civil and Environmental Engineering, King Fahd University of Petroleum & Minerals, 31261 Dhahran, Eastern Province, Saudi Arabia*

(*Received November 2, 2021, Revised November 8, 2022, Accepted November 17, 2022*)

Abstract. In this study, free vibration analysis of functionally graded (FG) porous truncated conical shell panels reinforced by graphene platelets (GPLs) has been investigated for the first time. Additionally, the effect of three different types of porosity distribution and five different types of GPLs patterns on dynamic response of the shell are also studied. Halpin-Tsai micromechanical model and Voigt's rule are used to determine Young modulus, shear modulus and Poisson's ratio with mass densities of the shell, respectively. The main novelties of present study are: applying 3D elasticity theory and the finite element method in conjunction with Rayleigh-Ritz method to give more accurate results unlike other simplified shell theories, and also presenting a general 3D solution in cylindrical coordinate system that can be used for analyses of different structures such as circular, annular and annular sector plates, cylindrical shells and panels, and conical shells and panels. A convergence study is performed to justify the correctness of the obtained solution and numerical results. The impact of porosity and GPLs patterns, the volume of voids, the weight fraction of graphene nanofillers, semi vertex and span angles of the cone, and various boundary conditions on natural frequencies of the functionally graded panel have been comprehensively studied and discussed. The results show that the most important parameter on dynamic response of FG porous truncated conical panel is the weight fraction of nanofiller and adding 1% weight fraction of nanofiller could increase 57% approximately the amounts of natural frequencies of the shell. Moreover, the porosity distribution has great effect on the value of natural frequency of structure rather than the porosity coefficient.

Keywords: FEM; graphene platelets; porosity; truncated conical shell panel; vibration; 3-D elasticity

1. Introduction

Recently, there is a high demand for great structural implementation and multifunctionality with excellent mechanical properties. The porous structures reinforced by graphene platelet (GPLs) having valuable properties, such as heat resistance, lightweight, and excellent energy absorption, have been considerably used in different engineering implementations. However, the stiffness of porous structures reduces significantly, due to the internal cavities, by adding GPLs into porous medium so effective mechanical properties of these structures considerably compensate. Many investigations have been performed about the behavior of FG porous structures reinforced by GPLs. However, studies on dynamic responses of these structures are limited, some of which are mentioned below.

Kitipornchai *et al*. (2017) used Ritz method to perform an investigation related to natural frequency and elastic buckling analyses of FG porous beams reinforced by GPLs based on Timoshenko beam theory. Yang *et al*. (2020) studied thermo-mechanical vibration of FG curved nanobeam contained porosities and reinforced with GPLs based on a shear deformation beam theory associated with the nonlocal strain gradient theory. Zhang *et al*. (2021) employed the DSC regularized Dirac-delta method for dynamic analysis of FG-GPL porous beams resting on the elastic foundation and subjected to moving load. Priyanka *et al*. (2021) studied the influence of graded porosity, GPLs, and axially varying loads on stability and dynamic response of beams. Binh *et al*. (2021) used the generalized differential quadrature method (GDQM) to study free vibration of rotating FG porous beams reinforced by GPLs based on Timoshenko beam theory. Xu *et al*. (2021) investigated free vibration of FG-GPL porous beams based on Euler–Bernoulli beam theory with spinning movement by applying the differential transformation method (DTM). Dynamic characteristics of FG-GPL porous nanocomposite curved beams modeled based on the trigonometric shear deformation theory were presented by Ganapathi *et al*. (2021). Yas and Rahimi (2020) used GDQM to study thermal vibration of FG porous beam reinforced by GPLs

*Corresponding author, Assistant Professor,
E-mail: xialingqin@zime.edu.cn
**Co-corresponding author, Assistant Professor,
E-mail: K.asemi@iau-tnb.ac.ir; kamiran64@yahoo.com
***Co-corresponding author, Professor,
E-mail: tou_abdel@yahoo.com

ISSN: 2287-237X (Print), 2287-2388 (Online)

based on Timoshenko beam theory. Safarpour *et al*. (2021b) applied GDQM to perform a parametric 3D study for bending and free vibration of FG-GPL porous circular and annular plates with various boundary conditions. Nguyen *et al*. (2020) presented a novel computational approach to investigate free vibration and static bending analysis of FG-GPL porous plates based on the first shear deformation theory (FSDT) and polygonal mesh with serendipity type shape functions. Gao *et al*. (2018) analyzed nonlinear free vibration of porous nanocomposite plates resting on the elastic foundation based on the classical plate theory (CPT) with the consideration of nonlinear von Kármán assumptions. The governing equations were solved by employing DQM. Based on FSDT, an analytical investigation regarding vibration and stability analyses of FG-GPL porous plates under aerodynamical loading was performed by Saidi *et al*. (2019). Asemi *et al*. (2020) comprehensively investigated static, free and forced vibration of FG porous annular sector plate reinforced by GPLs based on the FSDT. Rayleigh-Ritz energy formulation was applied to achieve the governing equations of motion, and FEM was employed to solve the derived equations. Phan (2020) presented isogeometric analysis of free and forced vibration analysis of FG-GPL porous plates using a refined plate theory via employing the non-uniform rational B-splines (NURBS). Gao *et al*. (2020) investigated wave propagation in FG porous plates reinforced with GPLs. The governing equations of wave propagation are derived by Hamilton's principle using assumptions of different plate theories. Zhou *et al*. (2020) investigated free vibration of FG-GPL porous plates applying 3D theory of elasticity and generalized DQM to derive and solve the governing motion equations. Teng and Wang (2021) studied nonlinear forced vibration of simply supported FG porous nanocomposite thin plates reinforced with GPLs based on CPT. They applied Galerkin method to solve the formulated boundary value problem. Based on the FSDT and Chebyshev polynomials, a novel quadrilateral element for analysis of FG porous plates/shells reinforced by GPLs was presented by Ton-That *et al*. (2021). Ansari *et al*. (2021) presented a novel solution according to variational differential quadrature (VDQ) for free vibration analysis of post-buckled arbitrary-shaped FG-GPL-reinforced porous nanocomposite plates based upon the third-order shear deformation theory (TSDT).

The above literature review shows that the major portion of investigations is related to beam and plate-type structures and limited investigations have been performed about dynamic response of FG porous shell-type structures reinforced by GPLs. For instance, Safarpour *et al*. (2020) investigated three-dimensional static and free vibration analyses of FG-GPL truncated conical shells, cylindrical shells and annular plates with various boundary conditions within the framework of elasticity theory. Bahaadini *et al*. (2019) presented an analytical solution for free vibration of FG-GPL porous truncated conical shell based on the Love's first approximation theory. The effects of porosity coefficient, geometry and weight fraction of GPLs on the natural frequencies have been examined. A review paper on FG porous structures reinforced by graphene platelet was performed by Kiarasi *et al*. (2022). Ye and Wang (2021) investigated the internal resonance of FG-GPL reinforced metal foam cylindrical shells based on Donnell's nonlinear shell theory and by using Galerkin method. Wang *et al*. (2019) employed Galerkin method to study the nonlinear vibration of metal foam cylindrical shells reinforced with GPLs based on improved Donnell's nonlinear shell theory. Moradi Dastjerdi and Behdinan (2021) studied stress waves in thick porous graphene-reinforced cylinders under thermal gradient environments by applying the moving least squares (MLSs) interpolation functions. Salehi *et al*. (2021) presented an analytical solution for nonlinear vibration of shear deformable imperfect FG-GPL porous nanocomposite cylindrical shells based on FSDT. Nejadi *et al*. (2021 a) employed GDQM to investigate natural frequencies of sandwich pipe by considering porosity and GPL effects on conveying fluid flow. Zhou *et al*. (2021) studied vibration and flutter characteristics of GPL-reinforced functionally graded porous cylindrical panels subjected to supersonic flow based on Reddy's TSDT and by applying the standard Lagrange procedure. Ebrahimi *et al*. (2019) performed vibration analysis of FG porous shells reinforced by GPLs based on the FSDT. Pourjabari *et al*. (2019) performed an investigation related to effect of porosity on the free and forced vibration characteristics of the GPL reinforcement composite cylindrical microshell based on the modified strain gradient theory (MSGT). Baghlani *et al*. (2021) studied free vibration of functionally graded graphene-reinforced porous nanocomposite shells of revolution based on the HSDT and by using Fourier Differential Quadrature (FDQ) technique. In another investigation (Khayat *et al*. 2021), based on the same solution, they studied nonlinear dynamic responses of smart sandwich FG porous cylindrical shells reinforced by GPLs under rectangular, sine, and exponential loads. Kargar *et al*. (2022) investigated dynamic bending analysis of laminated porous concrete beam reinforced by nanoparticles based on sinusoidal shear deformation theory and by employing DQM. Cui *et al*. (2022) employed DQM to investigate the nonlinear vibration behavior of nanocomposite sandwich panel based on shell theories. The literature review shows that: 1- Most of the studies are relevant to the behavior of FG-GPL porous plate-type structures and beams. However, less attention has been paid to investigating the behavior of FG-GPL porous shells. 2- Among shell-type structures, natural frequencies of FG porous truncated conical shell panels have not been investigated, so far. 3- Analyses have been mainly performed based on the ESL plate and shell theories rather than elasticity theory. Due to the wide application of conical panel-like shapes as a part of complex structures in the aerospace industry (Khakimova *et al*. 2016, Zhang and Cao 2022), it is necessary to know the free vibration behavior of these structures made of lightweight nanomaterial such as FG–GPL porous materials. Hence, in this research, free vibration analysis of truncated conical panels made of FG porous reinforced by GPLs is investigated for the first time. The truncated conical panels are considered with uniform and non-uniform patterns of GPLs in a metallic matrix containing open-cell internal pores as well as three various porosity

distributions that are assumed across the thickness of the shell. Porosity is assumed as uniformly and nonlinearly distributed. In addition, five various patterns of GPL dispersion pattern are assumed through the shell thickness. 3-D elasticity theory in conjunction with the finite element method based on Rayleigh-Ritz procedure is applied to obtain and solve the governing equations. The main novelties of present study are: 1- Applying 3D elasticity theory which considers thickness stretching effect and gives more accurate results unlike other simplified shell theories. Shell theories underpredict displacements and natural frequencies of thick shells. 2- The displacement varies along with the thickness, and it is appropriate for thick structures, especially including material properties variation across their whole thickness.3- A general 3D elasticity solution in cylindrical coordinate is presented that can be used for analyses of different structures such as circular, annular and annular sector plates, cylindrical shells and panels, and conical shells and panels. The influences of different factors such as porosity coefficient, various porosity distributions in conjunction with different GPL patterns, weight fraction of GPLs, semi vertex angle and span angle of the cone, and various boundary conditions on natural frequencies and mode shapes of the truncated conical panel have been comprehensively investigated.

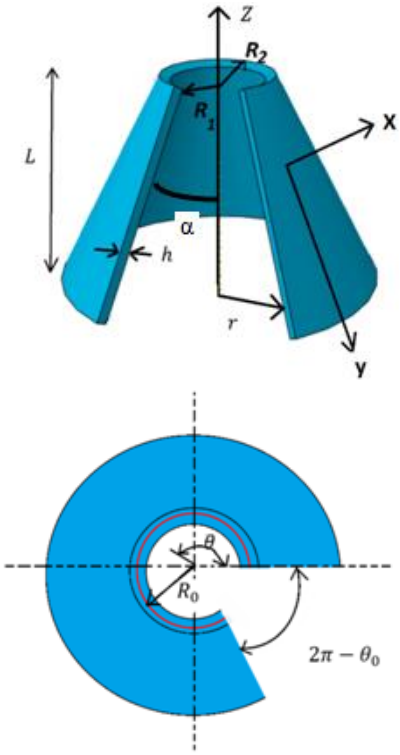

Fig. 1 Geometrical scheme of the FG porous truncated conical panel reinforced by GPLs

2. Theoretical formulations

2.1 Description of the geometry:

The truncated conical panel has inner radius $R_1 = a$, an outer radius $R_2 = b$ of the small base, span angle θ_0, semi vertex angle α and length L. The geometry of the shell defined in the cylindrical coordinates (r, θ, z) is presented in Fig. 1.

2.2 Estimating mechanical properties of the shell:

Many researchers studied the effect of different porosity distribution on behavior of a structure. Their results show that porosity distribution plays an important role to achieve the best static and dynamic performance and also to obtain the greatest energy absorption capability at low- and high-velocity impacts, respectively (Wu *et al*. 2020). Hence, in this study, three different popular porosity distributions are assumed through the truncated conical panel thickness (Fig. 2). Two types of non-uniform symmetric distributions of porosity and a uniform porosity distribution are considered. In distribution 1, the porosity is symmetric, nonlinear, and its distribution around the mid-surface is higher than around the inner and outer surfaces of the shell. In distribution 2, the porosity is also symmetric and nonlinear, but the porosity near the inner and outer surfaces is higher than around the mid-surface. The distribution of material properties including the effect of porosity with distributions 1, 2 and 3 are given in Fig. 2 (A, B, C), respectively. Besides, five GPL distribution patterns along the shell thickness are indicated in Fig. 2 (a-e) according with Salmani *et al*. (2021) and Mirjavadi *et al*. (2019). It should be noted that the material gradation is along the x axis (thickness direction). The mechanical properties including Young's modulus $E(\varsigma)$, shear modulus $G(\varsigma)$ and mass density $\rho(\varsigma)$ of porous nanocomposite shell are described as follows (Asemi *et al*. 2020, Babaei *et al*. 2020, 2021, Berghouti *et al*. 2019, Bouhadra *et al*. 2021, Huang *et al*. 2022, Cuong-Le *et al*. 2022, Behdinan 2022, Fenjan *et al*. 2020a, Al-Osta 2022): Porosity distribution 1 (Non-uniform symmetric I):

$$\begin{cases} E(\varsigma) = E^*[1 - e_0 \cos(\pi\varsigma)] \\ G(\varsigma) = G^*[1 - e_0 \cos(\pi\varsigma)] \\ \rho(\varsigma) = \rho^*[1 - e_m \cos(\pi\varsigma)] \end{cases} \quad (1)$$

where $\varsigma = x/h, -h/2 \le x \le h/2$,

Porosity distribution 2 (Non-uniform symmetric II):

$$\begin{cases} E(\varsigma) = E^*[e_0^*(1 - \cos(\pi\varsigma))] \\ G(\varsigma) = G^*[e_0^*(1 - \cos(\pi\varsigma))] \\ \rho(\varsigma) = \rho^*[e_m^*(1 - \cos(\pi\varsigma))] \end{cases} \quad (2)$$

Uniform porosity distribution:

$$\begin{cases} E(\varsigma) = E^*\gamma \\ G(\varsigma) = G^*\gamma \\ \rho(\varsigma) = \rho^*\gamma' \end{cases} \quad (3)$$

where E^*, G^* and ρ^* are the Young's modulus, shear modulus and mass density of truncated conical panel reinforced by GPLs and without interior cavities, respectively. Also, e_0 and e_0^* $(0 \le e_0(e_0^*) < 1)$ are the coefficients of porosity for distributions 1 and 2, respectively. e_m and e_m^* indicate the mass density coefficient for distributions 1 and 2, respectively. γ and γ'

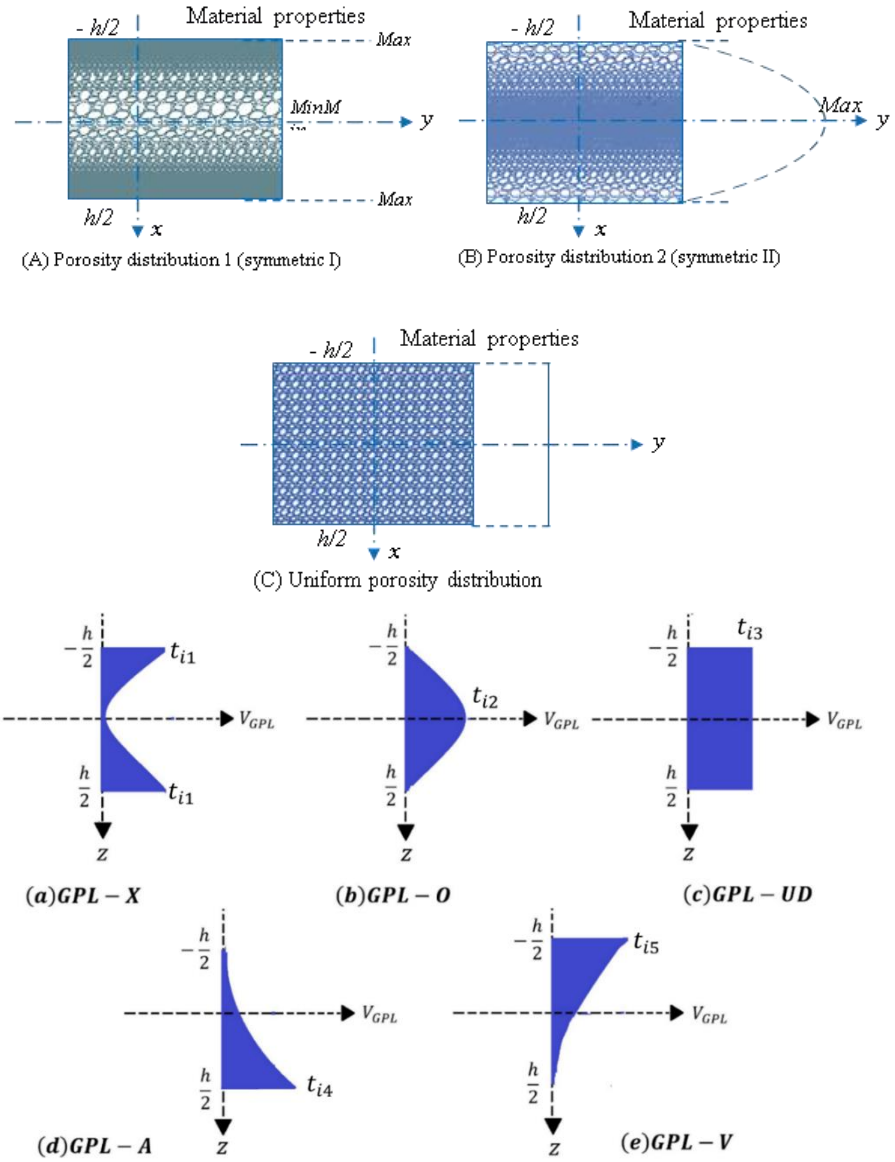

Fig. 2 Patterns of porosity and GPLs distributions along thickness of the shell

are the parameters of uniform porosity distribution. As the size and density of interior cavities increase, the porosity increases, and consequently, causes a reduction in the material properties.

The relation between Young's modulus and density for open-cell metal foams is presented as (Babaei *et al.* 2022, Arefi *et al.* 2021, Song *et al.* 2021, Amiri *et al.* 2021, Babaei *et al.* 2019, Fenjan *et al.* 2020b, Allah *et al.* 2022, Sokhandani *et al.*2022)

$$\frac{E(\varsigma)}{E^*} = \left(\frac{\rho(\varsigma)}{\rho^*}\right)^2 \tag{4}$$

Eq. (4) is utilized to derive the relation between the porosity coefficients and mass density coefficients for various porosity patterns as follows:

$$\begin{aligned} &1 - e_m cos(\pi) = \sqrt{1 - e_0 cos(\pi)} \\ &1 - e_m^*(1 - \cos(\pi\varsigma)) = \sqrt{1 - e_0^*(1 - \cos(\pi\varsigma))} \\ &\gamma^* = \sqrt{\gamma} \end{aligned} \tag{5}$$

Here, it is assumed that the mass of various plates with various porosity patterns and GPL dispersions are identical

$$\begin{aligned} &\int_0^{h/2} \sqrt{1 - e_0 \cos(\pi\varsigma)}\, d\varsigma = \\ &\int_0^{h/2} \sqrt{1 - e_0^*(1 - \cos(\pi\varsigma))}\, d\varsigma = \int_0^{h/2} \sqrt{\gamma}\, d\varsigma \end{aligned} \tag{6}$$

According to Eq (6), the values of e_0^* and γ can be estimated with a known value ofe_0, as given in Table 1. It is seen that e_0^* increases as e_0 increases. When e_0 is 0.6, e_0^* is calculated to be 0.9612 which is near to the upper bound. Thus, $e_0 \in [0,0.6]$ is used in this work.

The Halpin–Tsai model is commonly used to predict the effective stiffness (modulus of elasticity) for fiber reinforced composites with perfect fiber alignment and is more accurate way rather than the rule of mixture, because the effect of length and thickness of graphene nanoplatelets are successfully taken into account in the modified Halpin-Tsai equations. Hence, according to Halpin-Tsai micro-mechanical model (Gibson *et al.* 1982, Teng *et al.* 2021,

Ebrahimi and Hosseini 2020), the Young's modulus of the nanocomposites without interior cavities is expressed as:

$$E^* = \frac{3}{8}\left(\frac{1+\varepsilon_L^{GPL}\eta_L^{GPL}V_{GPL}}{1-\eta_L^{GPL}V_{GPL}}\right)E_m + \frac{5}{8}\left(\frac{1+\varepsilon_W^{GPL}\eta_W^{GPL}V_{GPL}}{1-\eta_W^{GPL}V_{GPL}}\right) \quad (7)$$

where

$$\varepsilon_L^{GPL} = \frac{2l_{GPL}}{t_{GPL}} \quad (8)$$

$$\varepsilon_W^{GPL} = \frac{2W_{GPL}}{t_{GPL}} \quad (9)$$

$$\eta_L^{GPL} = \frac{E_{GPL}-E_m}{E_{GPL}+\varepsilon_L^{GPL}E_m} \quad (10)$$

$$\eta_W^{GPL} = \frac{E_{GPL}-E_m}{E_{GPL}+\varepsilon_W^{GPL}E_m} \quad (11)$$

The indices m and GPL denote the properties of metallic matrix and GPLs, respectively. V_{GPL} is the volume content of GPLs and l_{GPL}, w_{GPL} and t_{GPL} are length, width and thickness of nanofiller platelets, respectively.

In contrast to the Halpin-Tsai model, the rule of mixture is used to predict the mass density, Poisson's ratio. Hence, the effect of dimensions of nanoparticles is not considered in this method, it is not accurate for estimation of modulus of elasticity of fiber reinforced nanocomposites. Employing the rule of mixture, the mass density and Poisson's ratio of the nanocomposite material are estimated as follows (Khatounabadi *et al*. 2022, Nejadi *et al*. 2021 b, Oskouie *et al*. 2021, Safarpour *et al*. 2021a, Ebrahimi and Dabbagh 2021, Zhou *et al*. 2022):

$$\rho^* = \rho_{GPL}V_{GPL} + \rho_m(1-V_{GPL}) \quad (12)$$

$$v^* = V_{GPL}V_{GPL} + V_m(1-V_{GPL}) \quad (13)$$

The $G*$ shear modulus is expressed as:

$$G^* = \frac{E^*}{2(1+v^*)} \quad (14)$$

The volume content of GPLs, V_{GPL}, is assumed to change across the truncated conical panel thickness (x direction) with five dispersion patterns (see also Fig. (2)):

$$V_{GPL}(x) = \begin{cases} t_{i1}[1-\cos(\pi\varsigma)] & GPL-X \\ t_{i2}[\cos(\pi\varsigma)] & GPL-0 \\ t_{i3} & GPL-UD \\ t_{i4}\left[1-\cos(\frac{\pi}{4}-\frac{\pi}{2}\varsigma)\right] & GPL-A \\ t_{i5}\left[\cos(\frac{\pi}{4}-\frac{\pi}{2}\varsigma)\right] & GPL-V \end{cases} \quad (15)$$

where $t_{i1}, t_{i2}, t_{i3}, t_{i4}$ and t_{i5} denote the upper limit of the V_{GPL}, and subscript $i = 1,2,3$ denotes various porosity distributions 1, 2 and 3 within each pattern. V_{GPL}^T is the total volume content of GPLs and is estimated by applying the nanofiller weight fraction Δ_{GPL} into Eq.(16), then it is used to derive $t_{i1}, t_{i2}, t_{i3}, t_{i4}$ and t_{i5} by Eq. (17) (Kiarasi *et al*. 2021)

Table 1 Porosity coefficients for different distributions

e_0	e_0^*	γ
0.1	0.1738	0.9361
0.2	0.3442	0.8716
0.3	0.5103	0.8064
0.4	0.6708	0.7404
0.5	0.8231	0.6733
0.6	0.9612	0.6047

$$V_{GPL}^T = \frac{\Delta_{GPL}\,\rho_m}{\Delta_{GPL}\,\rho_m + \rho_{GPL} - \Delta_{GPL}\,\rho_{GPL}} \quad (16)$$

$$V_{GPL}^T = \int_{-h/2}^{h/2}\frac{\rho(\varsigma)}{\rho_c}dz = \begin{cases} t_{i1}\int_{-h/2}^{h/2}[1-\cos(\pi\varsigma)]\frac{\rho(\varsigma)}{\rho_c}d\varsigma \\ t_{i2}\int_{-h/2}^{h/2}[\cos(\pi\varsigma)]\frac{\rho(\varsigma)}{\rho_c}d\varsigma \\ t_{i3}\int_{-h/2}^{h/2}\frac{\rho(\varsigma)}{\rho_c}d\varsigma \\ t_{i4}\int_{-h/2}^{h/2}\left[1-\cos(\frac{\pi}{4}-\frac{\pi}{2}\varsigma)\right]\frac{\rho(\varsigma)}{\rho_c}d\varsigma \\ t_{i5}\int_{-h/2}^{h/2}\left[\cos(\frac{\pi}{4}-\frac{\pi}{2}\varsigma)\right]\frac{\rho(\varsigma)}{\rho_c}d\varsigma \end{cases} \quad (17)$$

2.3 Constitutive relations

The stress-strain relationships according to Hooke's law in cylindrical coordinates are as follows:

$$[\sigma]_{r,\theta,z} = D[\varepsilon]_{r,\theta,z} \quad (18)$$

In the above equations $[\sigma]$ is the stress matrix, D is the matrix of elastic constants, and $[\varepsilon]$ is the strain matrix. Matrix $[D]$ is defined as:

$$D = \frac{E(x)(1-v)}{(1+v)(1-2v)}\begin{pmatrix} 1 & \frac{v}{1-v} & \frac{v}{1-v} & 0 & 0 & 0 \\ \frac{v}{1-v} & 1 & \frac{v}{1-v} & 0 & 0 & 0 \\ \frac{v}{1-v} & \frac{v}{1-v} & 1 & 0 & 0 & 0 \\ 0 & 0 & 0 & \frac{1-2v}{2(1-v)} & 0 & 0 \\ 0 & 0 & 0 & 0 & \frac{1-2v}{2(1-v)} & 0 \\ 0 & 0 & 0 & 0 & 0 & \frac{1-2v}{2(1-v)} \end{pmatrix} \quad (19)$$

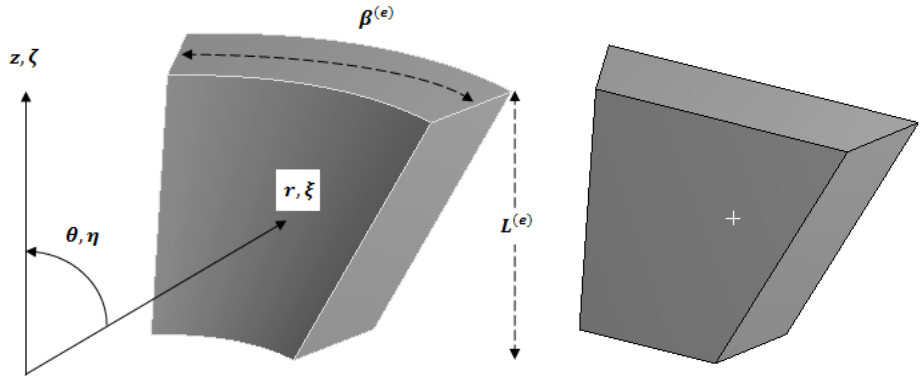

Fig. 3 Schematic of 8 node brick element and local coordinates system

The strain-displacement relationships in the cylindrical coordinates are

$$\varepsilon_r = \frac{\partial u}{\partial r}\ ,\ \gamma_{\theta z} = \frac{\partial v}{\partial z} + \frac{1}{r}\frac{\partial w}{\partial \theta}$$
$$\varepsilon_\theta = \frac{1}{r}\left(u + \frac{\partial v}{\partial \theta}\right),\ \gamma_{rz} = \frac{\partial u}{\partial z} + \frac{\partial w}{\partial r} \quad (20)$$
$$\varepsilon_z = \frac{\partial w}{\partial z}\ ,\ \gamma_{r\theta} = \frac{1}{r}\frac{\partial u}{\partial \theta} + \frac{\partial v}{\partial r} - \frac{v}{r}$$

The relation between local and global coordinates is presented in the following way:

$$\xi = \left(2r - a^{(e)} - b^{(e)}\right)/\left(b^{(e)} - a^{(e)}\right),$$
$$\eta = 2\theta/\beta^{(e)},\ \zeta = 2z/L^{(e)} \quad (21)$$

In the above relations $-1 \le \xi,\ \eta$ and $\zeta \le 1$ and $a^{(e)}, b^{(e)}, L^{(e)},\ \beta^{(e)}$ are the inner radius, outer radius, length (z direction) and span angle of each element in the solution domain, respectively (Fig. 3).

According to the above relations, the strain relation can be rewritten in the following form:

$$d = \begin{bmatrix} \frac{\partial}{\partial \xi}\frac{2}{b^{(e)} - a^{(e)}} & 0 & 0 \\ \frac{2}{\xi(b^{(e)} - a^{(e)}) + a^{(e)} + b^{(e)}} & \frac{4}{\xi(b^{(e)} - a^{(e)}) + a^{(e)} + b^{(e)}}\frac{\partial}{\beta^{(e)}\partial \eta} & 0 \\ 0 & 0 & \frac{2\partial}{L^{(e)}\partial \zeta} \\ \frac{4}{\xi(b^{(e)} - a^{(e)}) + a^{(e)} + b^{(e)}}\frac{\partial}{\beta^{(e)}\partial \eta} & \frac{\partial}{\partial \xi}\frac{2}{b^{(e)} + a^{(e)}} - \frac{2}{\xi(b^{(e)} - a^{(e)}) + a^{(e)} + b^{(e)}} & 0 \\ 0 & \frac{2\partial}{L^{(e)}\partial \zeta} & \frac{4}{\xi(b^{(e)} - a^{(e)}) + a^{(e)} + b^{(e)}}\frac{\partial}{\beta^{(e)}\partial \eta} \\ \frac{2\partial}{L^{(e)}\partial \zeta} & 0 & \frac{\partial}{\partial \xi}\frac{2}{b^{(e)} - a^{(e)}} \end{bmatrix} \quad (22a)$$

$$q = \begin{Bmatrix} u \\ v \\ w \end{Bmatrix} \quad (22b)$$

where q is the displacement vector.

3. The 3-D finite element modeling

Three-dimensional eight node brick element is employed for the finite element analysis (Fig 3). Assuming the displacement vector of any desired point of the element can be extracted in the finite element using the following equation:

$$q = N\delta^{(e)} \quad (24)$$

In the above relation, $\boldsymbol{\delta}^{(e)}$ is the node displacement vector and N is the matrix of the shape functions

$$\delta^{(e)} = \{U_1\ V_1\ W_1 \ldots U_8\ V_8\ W_8\}^T \quad (25)$$

$$N = \begin{bmatrix} N_1 & 0 & 0 & N_2 & 0 & 0 & \ldots & N_8 & 0 & 0 \\ 0 & N_1 & 0 & 0 & N_2 & 0 & \ldots & 0 & N_8 & 0 \\ 0 & 0 & N_1 & 0 & 0 & N_2 & \ldots & 0 & 0 & N_8 \end{bmatrix}_{3*24} \quad (26)$$

The shape function based on the local coordinates is defined as:

$$N_i(\xi, \eta, \zeta) = \frac{1}{8}(1 + \xi_i\xi)(1 + \eta_i\eta)(1 + \zeta_i\zeta) \quad (27)$$

According to the above relation, the strain-displacement relation may be rewritten as follows:

$$\varepsilon^{(e)} = dN\delta^{(e)} = B\delta^{(e)} \quad (28)$$

The matrix B in the above relation is as the following form:

$$B = \begin{pmatrix} \frac{\xi_1(1+\eta_1\eta)(1+\zeta_1\zeta)}{4(b^{(e)}-a^{(e)})} & 0 & 0 & \dots \\ \frac{(1+\xi_1\xi)(1+\eta_1\eta)(1+\zeta_1\zeta)}{4(\xi(b^{(e)}-a^{(e)})+a^{(e)}+b^{(e)})} & \frac{\eta_1(1+\xi_1\xi)(1+\zeta_1\zeta)}{2\beta^{(e)}(\xi(b^{(e)}-a^{(e)})+a^{(e)}+b^{(e)})} & 0 & \dots \\ 0 & 0 & \frac{\xi_1(1+\xi_1\xi)(1+\eta_1\eta)}{4L^{(e)}} & \dots \\ \frac{\eta_1(1+\xi_1\xi)(1+\zeta_1\zeta)}{2\beta^{(e)}(\xi(b^{(e)}-a^{(e)})+a^{(e)}+b^{(e)})} & \frac{\xi_1(1+\eta_1\eta)(1+\zeta_1\zeta)}{4(b^{(e)}-a^{(e)})} - \frac{(1+\xi_1\xi)(1+\eta_1\eta)(1+\zeta_1\zeta)}{4(\xi(b^{(e)}-a^{(e)})+a^{(e)}+b^{(e)})} & 0 & \dots \\ 0 & \frac{\zeta_1(1+\xi_1\xi)(1+\eta_1\eta)}{4L^{(e)}} & \frac{\eta_1(1+\xi_1\xi)(1+\zeta_1\zeta)}{2\beta^{(e)}(\xi(b^{(e)}-a^{(e)})+a^{(e)}+b^{(e)})} & \dots \\ \frac{\zeta_1(1+\xi_1\xi)(1+\eta_1\eta)}{4L^{(e)}} & 0 & \frac{\xi_1(1+\eta_1\eta)(1+\zeta_1\zeta)}{4(b^{(e)}-a^{(e)})} & \dots \end{pmatrix}_{6^*24} \quad (29)$$

The governing equations of the FE model will be estimated based on the principle of minimum potential energy and Rayleigh–Ritz method, in which case the model potential energy by substituting Eqs. (24) and (28) in Eq. (30) will be expressed as follows:

$$\begin{aligned} \Pi^{(e)} &= \frac{1}{2}\int_{V^{(e)}} (\varepsilon)^T \sigma \, dV + \int_{V^{(e)}} \rho \, q^T \ddot{q} \, dV \\ &= \frac{1}{2}\int_{V^{(e)}} \left(B\delta^{(e)}\right)^T D \, B\delta^{(e)} \, dV + \int_{V^{(e)}} \rho\left(N\delta^{(e)}\right)^T (N \, \ddot{\delta^{(e)}}) \, dV \end{aligned} \quad (30)$$

In the above relations, A and $V^{(e)}$ are the volume and area of the element, respectively, so, based on the principle of minimum energy, we will have

$$\begin{aligned} &\frac{\partial \Pi^{(e)}}{\partial (\delta^{(e)})^T} = 0 \\ &\rightarrow \int_{V^{(e)}} \mathrm{B}^T D B \delta^{(e)} \, dV + \int_{V^{(e)}} \rho N^T (N \, \ddot{\delta^{(e)}}) \, dV = 0 \end{aligned} \quad (31)$$

Eq. (31) can be rewritten in the following form:

$$M^{(e)}\ddot{\delta}^{(e)} + K^{(e)}\delta^{(e)} = 0 \quad (32)$$

$$K^{(e)} = \int_{V^{(e)}} \mathrm{B}^T D B \, dV \quad (33)$$

$$M^{(e)} = \int_{V^{(e)}} \rho \mathrm{N}^T N \, dV \quad (34)$$

The mass and stiffness matrices are calculated using Gauss's 8-point numerical integration rules. By assembling the mass and stiffness matrices of each matrix element, the mass and stiffness geometry of the problem will be obtained. Final characteristic equation has the form:

$$M\ddot{\delta} + K\delta = 0 \quad (35)$$

Vibration analysis of the FG-GPL porous conical panel will be performed by using the following equation:

$$(K - M\omega^2)\delta = 0 \quad (36)$$

where the ω is the circular natural frequency and δ is the mode shapes.

In this research, two different boundary conditions have been considered as the following:

Case 1: Upper and lower base of cone are clamped:

$$u, v, w(r, \theta, z = 0, L) = 0 \quad (37)$$

Table 2 Convergence study of fundamental natural frequency for porous FG-GPL truncated conical panel $\left(a = 0.25\ m, b = 0.3\ m, L = 0.5\ m, \alpha = 45^\circ, \theta_0 = 90^\circ, PD1,\ e0 = 0.4,\ \gamma = 0.01 wt\%\ GPLX, BCs: Case\ 1\right)$

Number of elements $(n_r^{(e)}, n_\theta^{(e)}, n_z^{(e)})$	3*38*24	5*38*24	7*38*24	8*38*24
Ω	602.8	594.3	580.1	579.56

Case 2: Two straight surfaces of cone are clamped:

$$u, v, w(r, \theta = 0, \theta_0, z) = 0 \quad (38)$$

4. Numerical results

In this section, the results of free vibration analysis of FG-GPL porous truncated conical panel with two types of boundary conditions. Effects of diverse volume weight fraction of GPLs, GPL distribution patterns, porosity distribution, and porosity coefficient as well as various span angles and semi-vertex angles on eigenfrequencies and eigenmodes of the conical panel are investigated.

4.1 Convergence study

In this section, first of all, the convergence study of present results will be performed. After that, for verification of obtained results, two examples will be presented. In the first example, by simplifying our numerical code, the porous FG-GPL truncated conical panel will be changed to an isotropic homogeneous truncated conical panel. To ensure the validity of obtained results for the functionally graded structure, example 2 will be presented.

The convergence of the present FE results is investigated by comparing results of successive refinement of the size of the element. In this regard, results are compared for meshes with adequate fixed number of θ-z plane elements but with various numbers of elements in the r direction. Results for fundamental natural frequency of FG porous truncated conical panel $(a = 0.25\ m, b = 0.3\ m, L = 0.5\ m, \alpha = 45^\circ, \theta_0 = 90^\circ, PD1, e_0 = 0.4, \gamma = 0.01 wt\%, GPLX)$ are reported in Table 2. As may be noted from the results listed in Table 1, it may be deduced that convergent results correspond to 8 elements in the r direction.

Table 3 The comparison between present results (Hz) and ANSYS WORKBENCH results for various semi vertex angles of isotropic homogeneous truncated conical panel

(α)	Boundary / Conditions	ω_1	ω_2	ω_3	ω_4	ω_5	ω_6
30°	CASE 1 (Ansys Workbench)	633.64	694.88	951.26	1441.	1530.2	1548.2
	CASE 1 (Present)	631.2	691.8	959.6	1435.5	1526.1	1544.1
	CASE 2 (Ansys Workbench)	725.46	759.6	1244.6	1379.4	1382.4	1641.4
	CASE 2 (Present)	724.3	757.05	1241.7	1375.08	1383.5	1644.2
45°	CASE 1 (Ansys Workbench)	373.59	415.55	586.37	815.39	912.15	929.56
	CASE 1 (Present)	373.04	414.1	583.02	817.2	911.1	923.9
	CASE 2 (Ansys Workbench)	357.88	421.14	679.23	764.7	817.76	994.78
	CASE 2 (Present)	358.02	420.2	677.2	762.08	812.5	990.07
60°	CASE 1 (Ansys Workbench)	919.94	1147.3	1260.1	1742.2	1858.9	1930.
	CASE 1 (Present)	918.2	1144.3	1262.2	1737.04	1852.1	1924.7
	CASE 2 (Ansys Workbench)	753.47	1140.9	1243.3	1383.3	1577.2	1716.6
	CASE 2 (Present)	752.02	1142.8	1247.2	1386.5	1578.2	1720.8

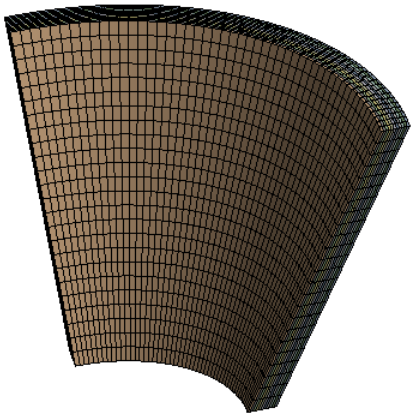

Fig. 4 The geometry and mesh model of the panel from ANSYS WORKBENCH

4.2 Validation of the present study

Example 1:

Due to the lack of published results about FG-GPL porous truncated conical panels, the results obtained in this study are verified with those of calculated from ANSYS WORKBENCH commercial FEM software. The meshed model is shown in Fig. 4. The material property and geometry of the truncated conical panel is assumed as follows:

Material property: $E = E_m = 130\ GPa$, $\rho = \rho_m = 8960\ kg/m^3$, $\upsilon = \upsilon_m$ 0.34

Geometry: $a = 0.25\ m, b = 0.3\ m, L = 0.5\ m, \alpha = 30^{\circ}, 45^{\circ}\ and\ 60^{\circ}, \theta_0 = 90°$

A comparison between the present and ANSYSY WORKBENCH results for various semi vertex angles of conical panel and different boundary conditions is shown in Table 3. This comparison shows an excellent agreement between them.

Example 2:

The free vibration of FG porous conical shells has been surveyed (Coung-Le *et al*. 2021). Hence, in this example, our results for FG porous truncated conical shell are obtained and compared with Coung-Le *et al*. (2021). For this target, the volume weight fraction of GPL will be zero ($\gamma = 0wt\%$). By this way, the porous FG-GPL structure will be changed to FG ones without nano-reinforcement. Besides, for verification our results with Coung-Le *et al*. (2021), the geometry and mechanical properties must be considered as follows:

Geometry:

$R_1 = 0.5, R_2 = 0.5 + L\ tan\alpha, h = 0.1\ m, L = 2\ m, \alpha = 40, \theta_0 = 360°$

Mechanical properties:

$\rho^* = 2126\frac{Kg}{m^3}$, $G^* = 7.608\ GPa, \nu = 0.15, E = 2G(1+\nu)$

The mechanical properties are varied through the thickness as the following:

$$E = E^*(1 - \eta(cos(\pi x/2h + \pi/4))$$
$$\rho = \rho^*(1 - \eta'(cos(\pi x/2h + \pi/4))$$
$$\eta' = \sqrt{1-\eta}$$

The dimensionless natural frequency is defined as $\overline{\omega} = \omega h\sqrt{\frac{\rho^*}{E^*}}$.

The comparison between obtained results and Coung-Le *et al*. (2021) shows excellent agreement.

4.3 Natural frequencies of FG-GPL porous truncated conical panel

In this section, the effect of semi vertex and span angles, two different types of boundary conditions, porosity coefficient and porosity distribution, GPL patterns and weight fraction of GPL nanofillers on natural frequencies of a truncated conical panel have been reported. Hence, the following material properties and geometrical parameters are considered:

Geometry: $a = 0.25\ m, b = 0.3\ m,$ L = 0.5 m, $\alpha = 30^0, 45^0, 60^0$, θ_0= 90º, 180º, 360º.

Material properties: $E_m = 130\ GPa, \rho_m = 8960\frac{kg}{m^3}$, $\nu_m =$ 0.34 or copper (Nejadi *et al*. 2021a), and $E_{GPL} = 1.01\ TPa$, $\rho_{GPL} = 1062.5\frac{kg}{m^3}$, $\nu_{GPL} = 0.186$, $W_{GPL} = 1.5\ \mu m$, $l_{GPL} = 2.5\ \mu m$, $t_{GPL} = 1.5\ nm$.

Table 4 Comparison of natural frequency Ω for C-F porous FG conical panel with various ratio of the radius to thickness and the porosity coefficient

R_1/h	2		5		10	
η	Coung-Le *et al*. (2021)	*Present*	Coung-Le *et al*. (2021)	*Present*	Coung-Le *et al*. (2021)	*Present*
0	0.7157	0.7255	0.4967	0.5063	0.3873	0.3938
0.1	0.7041	0.7172	0.4888	0.4969	0.3813	0.3870
0.3	0.6782	0.6918	0.4717	0.4781	0.3683	0.3758
0.5	0.6474	0.6579	0.4527	0.4574	0.3533	0.3606
0.7	0.6084	0.6147	0.4314	0.4407	0.3355	0.3386

Table 5 Natural frequencies (Hz) of FG-GPL porous shell for various boundary conditions and GPL patterns (α = 45˚, $\theta_0 = 90$˚, PD1, e_0=0.4, Υ_{GPL}=0.01wt%)

GPL pattern	BCs	ω_1	ω_2	ω_3	ω_4	ω_5	ω_6
GPL-X	CASE 1	579.56	640.8	882.12	1278.9	1410.8	1428.4
	CASE 2	561.82	615.31	1051.2	1117.8	1257.8	1554.9
GPL-A	CASE 1	433.08	482.31	678.85	940.39	1055	1075.7
	CASE 2	414.48	490	788.37	884.68	943.31	1154.2
GPL-V	CASE 1	390.07	434.42	612.17	846.06	950.16	968.94
	CASE 2	372.39	442.27	710.94	798.38	849.21	1034.9
GPL-O	CASE 1	395.87	440.97	636.88	847.41	960.04	982.79
	CASE 2	375.21	465.7	725.79	844.22	863.31	1040.5
GPL-UD	CASE 1	432.71	481.92	678.66	939.22	1054.1	1074.8
	CASE 2	414.09	490.15	787.95	884.9	942.59	1153.2

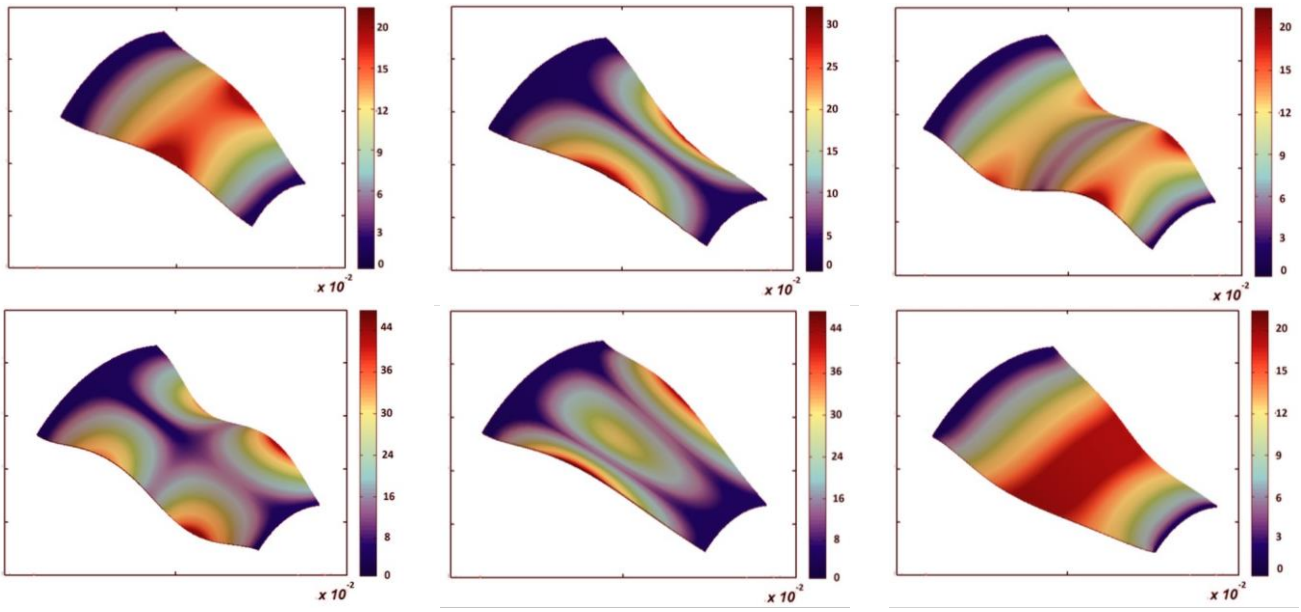

Fig. 5 The first six mode shapes of FG porous truncated conical panel reinforced by GPLs (α=30^0, θ_0=45^0, Case 1, GPL-X, PD1, e_0=0.4, Υ_{GPL}=0.01wt%)

Table 5 shows the effect of two types of boundary conditions and various GPL patterns on the natural frequencies of FG porous truncated conical panel reinforced by GPLs (α=45˚, $\theta_0 = 90$˚, PD1,e_0=0.4, Υ_{GPL}=0.01wt%). This table shows that for all the BCs, the maximum and minimum natural frequencies are related to GPLX and GPL-V, respectively. It means that when the GPL nano-fillers are more concentrated around the inner and outer surface of shell, the stiffness of shell is higher than for other types of GPL dispersion patterns. Also, when the GPL nanofillers are more dispersed around the outer surface of shell, the stiffness of shell has its minimum value. It is mentioned that the amount of natural frequencies for GPL-O and GPL-V are approximately the same. Moreover, this behavior can be seen for GPL-A and UD as well. This result can be very useful for the designers to apply these two

Table 6 Natural frequencies (Hz) of FG-GPL porous shell for various boundary condition and porosity distribution ($\alpha = 45^{\circ}$, $\theta_0 = 90^{\circ}$, GPLX, e_0=0.2, Υ_{GPL}=0.01wt%)

Porosity distribution	BCs	ω_1	ω_2	ω_3	ω_4	ω_5	ω_6
PD1	CASE 1	500.16	554.8	767.68	1099.2	1218	1236.2
	CASE 2	484	542.28	907.72	982.05	1087.5	1344
PD2	CASE 1	400.28	446.12	644.39	858.55	970.96	994.12
	CASE 2	379.98	471.77	735.91	856.12	875.53	1054.3
PD3	CASE 1	484.72	536.82	740.85	1067.2	1181.3	1197.4
	CASE 2	468.68	520.19	879.95	943.14	1053	1299.9

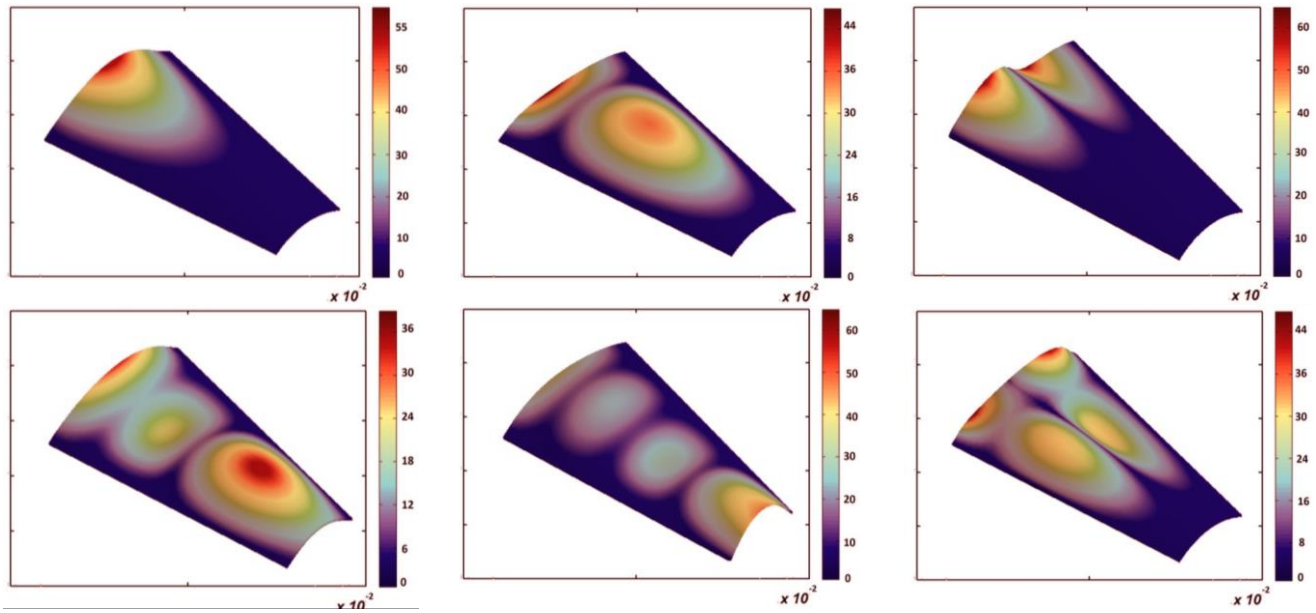

Fig. 6 The first six mode shapes of FG porous truncated conical panel reinforced by GPLs (α=30^0, θ_0=45^0, Case 2, GPL-X, PD1, e_0=0.4, Υ_{GPL}=0.01wt%)

Table 7 Natural frequencies (Hz) of FG-GPL porous shell for various boundary condition and weight fraction of GPL nano-fillers ($\alpha = 45^{\circ}$, $\theta_0 = 90^{\circ}$, PD1, e_0=0.4, GPLX)

Weight fraction of nano-fillers (%wt)	BCs	ω_1	ω_2	ω_3	ω_4	ω_5	ω_6
0%	CASE 1	368.12	408.34	565.39	807.65	897.49	910.9
	CASE 2	354.84	399.77	668.26	723.21	799.59	984.79
0.5%	CASE 1	471.01	520.14	714.86	1040.3	1145	1158.5
	CASE 2	457.35	496.25	853.24	902.76	1020.7	1262.5
1%	CASE 1	579.56	640.8	882.12	1278.9	1410.8	1428.4
	CASE 2	561.82	615.31	1051.2	1117.8	1257.8	1554.9

patterns instead of each other in particular conditions. In all cases, the panel with clamped edges at its two end bases (Case 1 boundary condition) has higher natural frequencies than the panel with clamped edges at its straight surfaces (Case 2 boundary condition).

The effect of two different boundary conditions and various porosity distributions are depicted in Table 6 ($\alpha = 45^{\circ}$, $\theta_0 = 90^{\circ}$, GPLX, e_0 = 0.2, Υ_{GPL} = 0.01 wt%). Table 6 illustrates that the maximum and minimum natural frequencies belong to PD1 and PD2, respectively. It means that for more porosities around the mid-thickness of shell, the ratio of stiffness to mass of shell and consequently natural frequency is significantly higher than the other porosity distributions. It can be seen that the difference between maximum and minimum fundamental natural frequency for different porosity distributions is approximately 25%. On the other hand, PD1 provides more rigidity, while PD2 considerably reduces the stiffness of truncated conical panel.

The influences of various boundary conditions and weight fraction of nano-fillers on natural frequencies of truncated conical panel (α=45°, $\theta_0 = 90^{\circ}$, PD1, e_0=0.4, GPLX) are

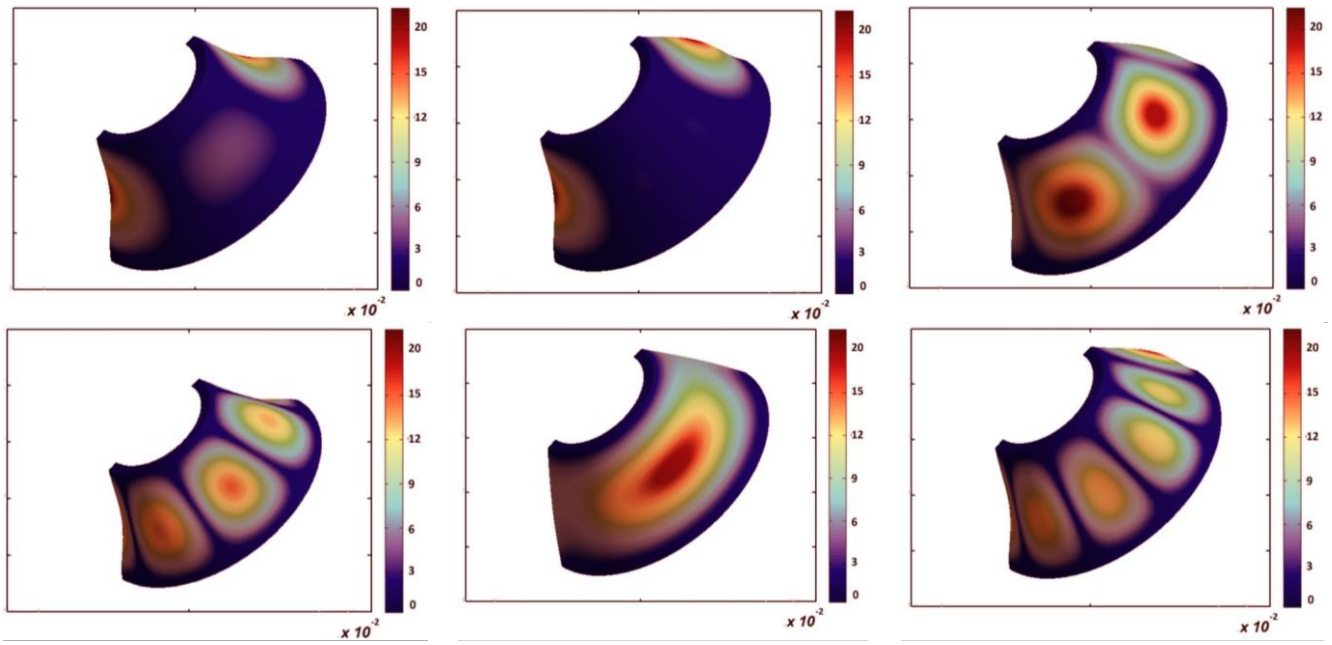

Fig. 7 The first six mode shapes of FG porous truncated conical panel reinforced by GPLs (α=30^0, θ_0=180^0, Case 1, GPL-X, PD1, e_0=0.4, Υ_{GPL}=0.01wt%)

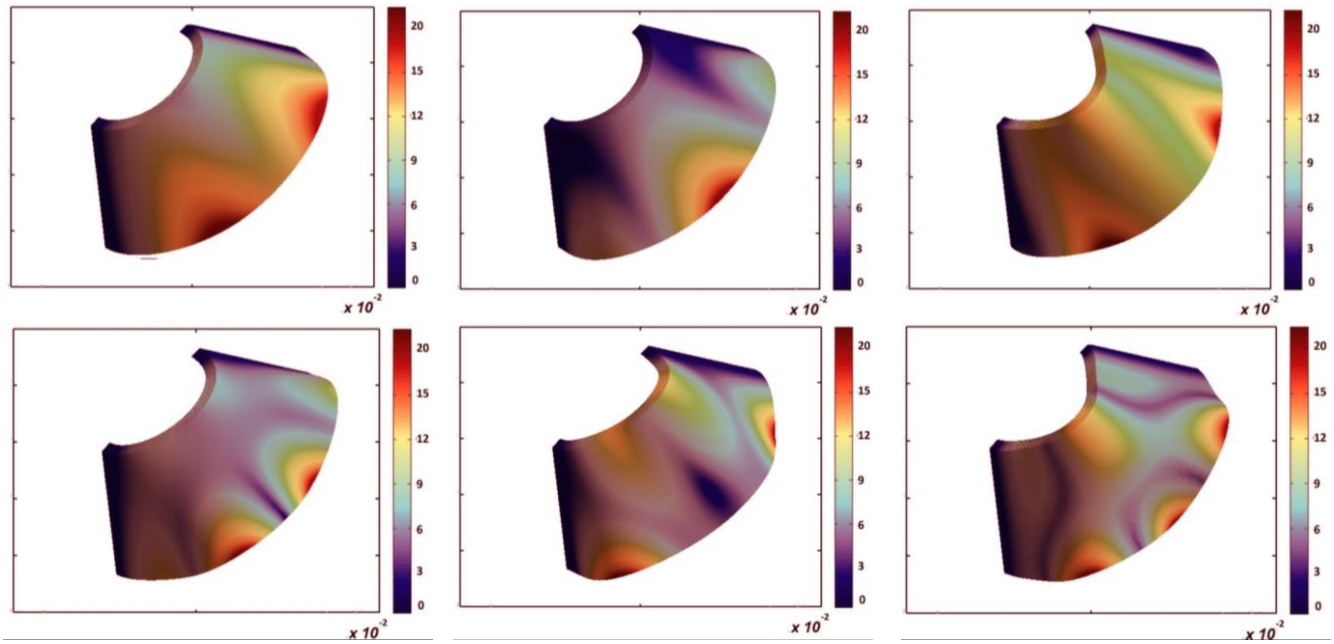

Fig. 8 The first six mode shapes of FG porous truncated conical panel reinforced by GPLs (α=30^0, θ_0=180^0, Case 2, GPL-X, PD1, e_0=0.4, Υ_{GPL}=0.01wt%)

Table 8 Natural frequencies of FG-GPL porous shell for various boundary condition and porosity coefficient (α = 45˚, θ_0 = 90˚, PD1, Υ_{GPL}=0.01wt%,GPLX)

e_0	BCs	ω_1	ω_2	ω_3	ω_4	ω_5	ω_6
0.2	CASE 1	500.16	554.8	767.68	1099.2	1218	1236.2
	CASE 2	484	542.28	907.72	982.05	1087.5	1344
0.4	CASE 1	579.56	640.8	882.12	1278.9	1410.8	1428.4
	CASE 2	561.82	615.31	1051.2	1117.8	1257.8	1554.9
0.5	CASE 1	590.17	682.13	933.14	1379.4	1594.12	1620.74
	CASE 2	578.22	641.83	1104.15	1227.16	1384.63	1700.45

Table 9 Natural frequencies of the structure for various boundary condition and semi-vertex angle ($\theta_0 = 90^\circ$, PD3, Υ_{GPL}=0.01wt%, GPL-UD, e_0=0.4)

Semi vertex angle (α)							
30°	CASE 1	734.1	806.11	1101.2	1661.2	1771.2	1792
	CASE 2	839.5	883.96	1438.6	1595.7	1601.4	1900.6
45°	CASE 1	432.71	481.92	678.66	939.22	1054.1	1074.8
	CASE 2	414.09	490.15	787.95	884.9	942.59	1153.2
60°	CASE 1	1078.5	1346.7	1478.	2017.8	2177.8	2213.7
	CASE 2	883.92	1331.5	1424.3	1621.7	1834.3	1989.3
	CASE 1	734.1	806.11	1101.2	1661.2	1771.2	1792

Table 10 Natural frequencies of FG-GPL porous shell for various boundary condition and span angle (α=30°, PD3, Υ_{GPL}=0.01wt%,GPL-UD, e_0=0.4)

Span angle (θ_0)	BCs	ω_1	ω_2	ω_3	ω_4	ω_5	ω_6
90	CASE 1	734.1	806.11	1101.2	1661.2	1771.2	1792
	CASE 2	839.5	883.96	1438.6	1595.7	1601.4	1900.6
180	CASE 1	762.21	769.99	1070.4	1162.1	1279.8	1444.5
	CASE 2	216.35	332.1	614.76	628.63	852.11	883.27
360	CASE 1	2251.6	2265.9	2456.5	2464.7	2611.7	2621.2
	CASE 1	734.1	806.11	1101.2	1661.2	1771.2	1792

given in Table 7. This table shows that by increasing the weight fraction of GPLs, the natural frequencies of structure considerably increase (approximately 57%), while the mass of structure changes a bit and this issue can be helpful for aerospace structures where the high stiffness and low density are so important.

Table 8 shows the effect of porosity coefficient on the natural frequencies of FG porous truncated conical panel reinforced by GPLs (α=45, $\theta_0 = 90$, PD1, Υ_{GPL}=0.01wt%, PLX). Results show that when the porosity of structure increases, the natural frequency of FG porous truncated cone reinforced by GPLs increases as well. This is due to the fact that by increasing the porosity, both the stiffness and mass of structure decrease, but the rate of reduction of mass is more than stiffness of structure. The effect of porosity coefficient on natural frequencies is lower than the effects of GPL pattern and weight fraction of nano-filler (its impact is approximately 18%). On the other hand, the effect of GPL pattern, porosity distribution, weight fraction of Nano-filler on the natural frequencies of FG porous truncated conical panel reinforced by GPL is more significant than porosity coefficient.

Table 9 shows the natural frequencies of shell for various boundary conditions and semi-vertex angle ($\theta_0 = 90^\circ$, PD3, Υ_{GPL}=0.01wt%, GPL-UD, e_0=0.4). This table denotes that the minimum and maximum natural frequencies are obtained respectively for α=45° and 60°. Also, the effect of various boundary condition and span angle are shown in Table 10 (α=30°, PD3, Υ_{GPL}=0.01 wt%, GPL-UD, e_0=0.4). As it can be seen from this table, by increasing the span angle of truncated conical panel, the natural frequencies enhance. Additionally, the first six mode shapes of FG porous truncated conical panels reinforced by GPLs are shown in Figs. 5-8 making completeness of this investigation.

4. Conclusions

Natural frequency analysis of FG porous truncated conical panel reinforced by graphene platelets has been investigated for the first time. Three different porosity distributions and five GPL patterns are considered along the shell thickness. Based on 3-D elasticity theory by employing FE and Rayleigh-Ritz methods, the governing equations of structure are obtained and numerically solved. The influences of GPL patterns, weight fraction of nanofillers, porosity coefficient, porosity distributions, semi vertex angle and span angle of the cone on the natural frequencies of panel have been studied and the main conclusions are below:

1. Maximum and minimum natural frequencies are related to GPL-X and GPL-V distributions, respectively.
2. The natural frequencies for GPL-X and FPL-V, and also for GPL-A and UD are almost the same.
3. The maximum and minimum natural frequencies belong to PD1 and PD2, respectively. Besides, the difference between maximum and minimum fundamental natural frequency for different porosity distributions is approximately 25%.
4. By increasing the weight fraction of GPLs, the natural frequencies of shell considerably increase (approximately 57%).
5. By increasing the porosity of shell, the natural frequencies increase about 18%.

Acknowledgements

This work was supported by Zhejiang Key Laboratory of Parts Rolling Technology (No. PR-22002), General Scientific Research Projects of Zhejiang Provincial Department of Education (NO. A-0275-21-059), Key

Research and Development Program of Zhejiang Province (No. 2022C01147), and Jianbing Lingyan Project (International Cooperation Project) of Zhejiang Province (2023c04050)

References

Allah, M.J., Timesli, A. and Belaasilia, Y. (2022), "Nonlinear dynamic analysis of porous functionally graded materials based on new third-order shear deformation theory", *Steel Compos. Struct.*, **43**(1), 1-17. https://doi.org/10.12989/scs.2022.43.1.001

Al-Osta, M.A. (2022), "Wave propagation investigation of a porous sandwich FG plate under hygrothermal environments via a new first-order shear deformation theory", *Steel Compos. Struct.*, **43**(1), 117-127. https://doi.org/10.12989/scs.2022.43.1.117.

Amiri, A., Mohammadimehr, M. and Rahaghi, M.I. (2021), "Vibration analysis of a micro-cylindrical sandwich panel with reinforced shape-memory alloys face sheets and porous core", *Eur. Phys. J. Plus*, **136**(8), 1-20. https://doi.org/10.1140/epjp/s13360-021-01763-8.

Ansari, R., Hassani, R., Gholami, R. and Rouhi, H. (2021), "Free vibration analysis of postbuckled arbitrary-shaped FG-GPL-reinforced porous nanocomposite plates", *Thin Wall. Struct.*, **163**, 107701. https://doi.org/10.1016/j.tws.2021.107701.

Arefi, M., Moghaddam, S.K., Bidgoli, E.M.R., Kiani, M. and Civalek, O. (2021), "Analysis of graphene nanoplatelet reinforced cylindrical shell subjected to thermo-mechanical loads", *Compos. Struct.*, **255**, 112924. https://doi.org/10.1016/j.compstruct.2020.112924.

Asemi, K., Babaei, M. and Kiarasi, F. (2020), "Static, natural frequency and dynamic analyses of functionally graded porous annular sector plates reinforced by graphene platelets", *Mech. Based Des. Struct.*, 1-29. https://doi.org/10.1080/15397734.2020.1822865.

Babaei, M., Asemi, K. and Kiarasi, F. (2020), "Static response and free-vibration analysis of a functionally graded annular elliptical sector plate made of saturated porous material based on 3D finite element method", *Mech. Based Des. Struct.*, 1-25. https://doi.org/10.1080/15397734.2020.1864401.

Babaei, M., Kiarasi, F. and Asemi, K, (2021), "Dynamic analysis of functionally graded rotating thick truncated cone made of saturated porous materials", *Thin Wall. Struct.*, **164**, 107852. https://doi.org/10.1016/j.tws.2021.107852.

Babaei, M., Kiarasi, F., Asemi, K., Dimitri, R. and Tornabene, F. (2022), "Transient thermal stresses in FG porous rotating truncated cones reinforced by graphene platelets", *Appl. Sci.*, **12**(8), 3932. https://doi.org/10.3390/app12083932.

Babaei, M., Safarpour, P. and Asemi, K. (2019), "Buckling and static analyses of functionally graded saturated porous thick beam resting on elastic foundation based on higher order beam theory", *Iran. J. Mech. Eng. Transact. ISME*, **20**(1), 94-112.

Baghlani, A., Najafgholipour, M.A. and Khayat, M. (2021), "The influence of mechanical uncertainties on the free vibration of functionally graded graphene-reinforced porous nanocomposite shells of revolution", *Eng. Struct.*, **228**, 111356. https://doi.org/10.1016/j.engstruct.2020.111356.

Bahaadini, R., Saidi, A.R., Arabjamaloei, Z. and Ghanbari-Nejad-Parizi, A. (2019), "Vibration analysis of functionally graded graphene reinforced porous nanocomposite shells", *Int. J. Appl. Mech.*, **11**(7), 1950068. https://doi.org/10.1142/S1758825119500686.

Behdinan, K. and Moradi-Dastjerdi, R. (2022), "Thermal buckling resistance of a lightweight lead-free piezoelectric nano-composite sandwich plate", *Adv. Nano Res.*, **12**(6), 593-603. https://doi.org/10.12989/anr.2022.12.6.593.

Berghouti, H., Adda Bedia, E. A., Benkhedda, A. and Tounsi, A. (2019), "Vibration analysis of nonlocal porous nanobeams made of functionally graded material", *Adv. Nano Res.*, **7**(5), 351-364. https://doi.org/10.12989/anr.2019.7.5.351.

Binh, C.T., Quoc, T.H., Huan, D.T. and Hien, H.T. (2021), "Vibration characteristics of rotating functionally graded porous beams reinforced by graphene platelets", *J. Sci. Technol. Civil Eng.*, ***15***(4), 29-41. https://doi.org/10.31814.

Bouhadra, A., Menasria, A. and Rachedi, M. A. (2021), "Boundary conditions effect for buckling analysis of porous functionally graded nanobeam", *Adv. Nano Res.*, **10**(4), 313-325. https://doi.org/10.12989/anr.2021.10.4.313.

Cui, Z., Cai, X., Ali, H.E. and Muhsen, S. (2022), "Investigating nonlinear vibration behavior of sandwich panels with multi-scale skins based on a numerical method", *Struct. Eng. Mech.*, **83**(3), 283-292. https://doi.org/10.12989/sem.2022.83.3.283.

Cuong-Le, T., Nguyen, K.D., Nguyen-Trong, N., Khatir, S., Nguyen-Xuan, H. and Abdel-Wahab, M. (2021), "A three-dimensional solution for free vibration and buckling of annular plate, conical, cylinder and cylindrical shell of FG porous-cellular materials using IGA", *Compos. Struct.*, **259**, 113216. https://doi.org/10.1016/j.compstruct.2020.113216.

Cuong-Le, T., Nguyen, K.D., Le-Minh, H., Phan-Vu, P., Nguyen-Trong, P. and Tounsi, A. (2022), "Nonlinear bending analysis of porous sigmoid FGM nanoplate via IGA and nonlocal strain gradient theory", *Adv. Nano Res.*, **12**(5), 441-455. https://doi.org/10.12989/anr.2022.12.5.441.

Ebrahimi, F., Seyfi, A., Dabbagh, A. and Tornabene, F. (2019), "Wave dispersion characteristics of porous graphene platelet-reinforced composite shells", *Struct. Eng. Mech.*, ***71***(1), 99-107. https://doi.org/10.12989/sem.2019.71.1.099.

Ebrahimi, F., Dabbagh, A. (2021), "An analytical solution for static stability of multi-scale hybrid nanocomposite plates", *Eng. Comput.*, **37**, 545-559. https://doi.org/10.1007/s00366-019-00840-y.

Ebrahimi, F. and Hosseini, S. H. S. (2020), "Resonance analysis on nonlinear vibration of piezoelectric/FG porous nano-composite subjected to moving load", *Eur. Phys. J. Plus*, **135**(2), 1-23. https://doi.org/10.1140/epjp/s13360-019-00011-4.

Fenjan, R.M., Ahmed, R.A., Hamad, L.B., Falleh, N.M. (2020a), "A review of numerical approach for dynamic response of strain gradient metal foam shells under constant velocity moving loads", *Adv. Comput. Des.*, **5**(4), 349-362. https://doi.org/10.12989/acd.2020.5.4.349.

Fenjan, R.M.,Hamad, L.B., Falleh, N.M. (2020b), "Mechanical-hygro-thermal vibrations of functionally graded porous plates with nonlocal and strain gradient effects", *Adv. Aircr. Spacecr. Sci.*, **7**(2), 169-186. https://doi.org/10.12989/aas.2020.7.2.169.

Ganapathi, M., Anirudh, B., Anant, C. and Polit, O. (2021), "Dynamic characteristics of functionally graded graphene reinforced porous nanocomposite curved beams based on trigonometric shear deformation theory with thickness stretch effect", *Mech. Adv. Mater. Struct.*, **28**(7), 741-752. https://doi.org/10.1080/15376494.2019.1601310.

Gao, K., Gao, W., Chen, D. and Yang, J. (2018), "Nonlinear free vibration of functionally graded graphene platelets reinforced porous nanocomposite plates resting on elastic foundation", *Compos. Struct.*, **204**, 831-846. https://doi.org/10.1016/j.compstruct.2018.08.013.

Gao, W., Qin, Z. and Chu, F. (2020), "Wave propagation in functionally graded porous plates reinforced with graphene platelets", *Aerosp. Sci. Technol.*, **102**, 105860. https://doi.org/10.1016/j.ast.2020.105860.

Gibson, I. J. and Ashby, M. F. (1982), "The mechanics of three-dimensional cellular materials", *Proceedings of the royal society of London. A. Mathematical and physical sciences*, **382**(1782),

43-59. https://doi.org/10.1098/rspa.1982.0088.
Huang, X., Shan, H., Chu, W. and Chen, Y. (2022), "Computational and mathematical simulation for the size-dependent dynamic behavior of the high-order FG nanotubes, including the porosity under the thermal effects", *Adv. Nano Res.*, **12**(1), 101-115. https://doi.org/10.12989/anr.2022.12.1.101.
Karegar, M., Bidgoli, M.R. and Mazaheri, H. (2022), "Dynamic bending analysis of laminated porous concrete beam reinforced by nanoparticles considering porosity effects", *Steel Compos. Struct.*, **40**(1), 129-137. https://doi.org/10.12989/scs.2022.43.1.129.
Khakimova, R., Wilckens, D., Reichardt, J., Zimmermann, R. and Degenhardt, R. (2016), "Buckling of axially compressed CFRP truncated cones: Experimental and numerical investigation", *Compos. Struct.*, **146**, 232-247. https://doi.org/10.1016/j.compstruct.2016.02.023.
Khatounabadi, M., Jafari, M. and Asemi, K. (2022), "Low-velocity impact analysis of functionally graded porous circular plate reinforced with graphene platelets", *Waves Random Complex Med.*, 1-27. https://doi.org/10.1080/17455030.2022.2091182.
Khayat, M., Baghlani, A. and Najafgholipour, M. A. (2021), "The propagation of uncertainty in the geometrically nonlinear responses of smart sandwich porous cylindrical shells reinforced with graphene platelets", *Compos. Struct.*, ***258***, 113209. https://doi.org/10.1016/j.compstruct.2020.113209.
Kiarasi, F., Babaei, M., Mollaei, S., Mohammadi, M. and Asemi, K. (2021), "Free vibration analysis of FG porous joined truncated conical-cylindrical shell reinforced by graphene platelets", *Adv. Nano Res.*, **11**(4), 361-380. https://doi.org/10.12989/anr.2021.11.4.361.
Kiarasi, F., Babaei, M., Sarvi, P., Mohammadi, Asemi, K., Hosseini, M. and Omidi Bidgoli, M (2022), "A review on functionally graded porous structures reinforced by graphene platelets", **52**(4), 731-750. https://doi.org/10.22059/JCAMECH.2021.335739.675.
Kitipornchai, S., Chen, D. and Yang, J. (2017), "Free vibration and elastic buckling of functionally graded porous beams reinforced by graphene platelets", *Mater. Des.*, **116**, 656-665. https://doi.org/10.1016/j.matdes.2016.12.061.
Mirjavadi, S.S., Forsat, M., Barati, M.R., Abdella, G.M., Afshari, B.M., Hamouda, A.M.S. and Rabby, S. (2019), "Dynamic response of metal foam FG porous cylindrical micro-shells due to moving loads with strain gradient size-dependency", *Eur. Phys. J. Plus*, **134**(5), 214. https://doi.org/10.1140/epjp/i2019-12540-3.
Moradi-Dastjerdi, R. and Behdinan, K. (2021), "Stress waves in thick porous graphene-reinforced cylinders under thermal gradient environments", *Aerosp. Sci. Technol.*, **110**, 106476. https://doi.org/10.1016/j.ast.2020.106476.
Nejadi, M.M., Mohammadimehr, M. and Mehrabi, M. (2021a), "Free vibration and stability analysis of sandwich pipe by considering porosity and graphene platelet effects on conveying fluid flow", *Alexandria Eng. J.*, **60**(1), 1945-1954. https://doi.org/10.1016/j.aej.2020.11.042.
Nejadi, M.M., Mohammadimehr, M. and Mehrabi, M. (2021b). "Free vibration and buckling of functionally graded carbon nanotubes/graphene platelets Timoshenko sandwich beam resting on variable elastic foundation", *Adv. Nano Res.*, **10**(6), 539-548. https://doi.org/10.12989/anr.2021.10.6.539.
Nguyen, N.V., Nguyen-Xuan, H., Lee, D. and Lee, J. (2020), "A novel computational approach to functionally graded porous plates with graphene platelets reinforcement", *Thin Wall. Struct.*, **150**, 106684. https://doi.org/10.1016/j.tws.2020.106684.
Oskouie, M.F., Hassanzadeh-Aghdam, M.K., Ansari, R. (2021), "A new numerical approach for low velocity impact response of multiscale-reinforced nanocomposite plates", *Eng. Comput.*, **37**, 713-730. https://doi.org/10.1007/s00366-019-00851-9.
Phan, D.H. (2020), "Isogeometric analysis of functionally-graded graphene platelets reinforced porous nanocomposite plates using a refined plate theory", *Int. J. Struct. Stabil. Dyn.*, **20**(7), 2050076. https://doi.org/10.1142/S0219455420500765.
Pourjabari, A., Hajilak, Z.E., Mohammadi, A., Habibi, M. and Safarpour, H. (2019), "Effect of porosity on free and forced vibration characteristics of the GPL reinforcement composite nanostructures", *Comput. Math. Appl.*, **77**(10), 2608-2626. https://doi.org/10.1016/j.camwa.2018.12.041
Priyanka, R., Twinkle, C. M. and Pitchaimani, J. (2021), "Stability and dynamic behavior of porous FGM beam: influence of graded porosity, graphene platelets, and axially varying loads", *Eng. Comput.*, 1-20. https://doi.org/10.1007/s00366-021-01478-5.
Safarpour, M., Ebrahimi, F., Habibi, M., Safarpour, H. (2021a), "On the nonlinear dynamics of a multi-scale hybrid nano-composite disk", *Eng. Comput.*, **37**, 2369-2388. https://doi.org/10.1007/s00366-020-00949-5.
Safarpour, M., Rahimi, A., Alibeigloo, A., Bisheh, H. and Forooghi, A. (2021b), "Parametric study of three-dimensional bending and frequency of FG-GPLRC porous circular and annular plates on different boundary conditions", *Mech. Based Des. Struct.*, **49**(5), 707-737. https://doi.org/10.1080/15397734.2019.1701491.
Safarpour, M., Rahimi, A. and Alibeigloo, A. (2020), "Static and free vibration analysis of graphene platelets reinforced composite truncated conical shell, cylindrical shell, and annular plate using theory of elasticity and DQM", *Mech. Based Des. Struct.*, **48**(4), 496-524. https://doi.org/10.1080/15397734.2019.1646137.
Saidi, A.R., Bahaadini, R. and Majidi-Mozafari, K. (2019), "On vibration and stability analysis of porous plates reinforced by graphene platelets under aerodynamical loading", *Compos. Part B Eng.*, **164**,778-799. https://doi.org/10.1016/j.compositesb.2019.01.074.
Salehi, M., Gholami, R. and Ansari, R. (2021), "Analytical solution approach for nonlinear vibration of shear deformable imperfect FG-GPLR porous nanocomposite cylindrical shells", *Mech. Based Des. Struct.*, 1-23. https://doi.org/10.1080/15397734.2021.1891096.
Salmani, R., Gholami, R., Ansari, R. and Fakhraie, M. (2021), "Analytical investigation on the nonlinear postbuckling of functionally graded porous cylindrical shells reinforced with graphene nanoplatelets", *Eur. Phys. J. Plus*, **136**(1), 1-19.
Sokhandani, N., Setoodeh, A., Zebarjad, M., Nikbin, K,. Wheatley, G., (2022), "The influence of nano-silica on the wear and mechanical performance of vinyl-ester/glass fiber nano-composites", *Adv. Nano Res.*, **13**(1), 97-111. https://doi.org/10.12989/anr.2022.13.1.097.
Song, J., Karami, B., Shahsavari, D. and Civalek, Ö. (2021), "Wave dispersion characteristics of graphene reinforced nano-composite curved viscoelastic panels", *Compos. Struct.*, **277**, 114648. https://doi.org/10.1016/j.compstruct.2021.114648.
Teng, M.W. and Wang, Y.Q. (2021), "Nonlinear forced vibration of simply supported functionally graded porous nanocomposite thin plates reinforced with graphene platelets", *Thin Wall. Struct.*, **164**, 107799. https://doi.org/10.1016/j.tws.2021.107799.
Ton-That, H.L., Nguyen-Van, H. and Chau-Dinh, T. (2021), "A novel quadrilateral element for analysis of functionally graded porous plates/shells reinforced by graphene platelets", *Arch. Appl. Mech.*, **91**(6), 2435-2466. https://doi.org/10.1007/s00419-021-01893-6.
Wang, Y.Q., Ye, C. and Zu, J.W. (2019), "Nonlinear vibration of metal foam cylindrical shells reinforced with graphene platelets", *Aerosp. Sci. Technol.*, **85**, 359-370. https://doi.org/10.1016/j.ast.2018.12.022.

Wu, H., Yang, J. and Kitipornchai, S. (2020), "Mechanical analysis of functionally graded porous structures: A review", *Int. J. Struct. Stabil. Dyn.*, **20**(13), 2041015. https://doi.org/10.1142/S0219455420410151.

Xu, H., Wang, Y. Q. and Zhang, Y. (2021), "Free vibration of functionally graded graphene platelet-reinforced porous beams with spinning movement via differential transformation method", *Arch. Appl. Mech.*, **91**(12), 4817-4834. https://doi.org/10.1007/s00419-021-02036-7.

Yang, X., Liu, H. and Ma, J. (2020), "Thermo-mechanical vibration of FG curved nanobeam containing porosities and reinforced by graphene platelets", *Microsyst. Technol.*, **26**, 2535-2551. https://doi.org/10.1007/s00542-020-04794-w.

Yas, M.H. and Rahimi, S. (2020), "Thermal vibration of functionally graded porous nanocomposite beams reinforced by graphene platelets", *Appl. Math. Mech.*, ***41***(8), 1209-1226. https://doi.org/10.1007/s10483-020-2634-6.

Ye, C. and Wang, Y.Q. (2021), "Nonlinear forced vibration of functionally graded graphene platelet-reinforced metal foam cylindrical shells: Internal resonances", *Nonlin. Dyn.*, **104**(3), 2051-2069. https://doi.org/10.1007/s11071-021-06401-7.

Zhang, R., Cao, Y., (2022), "Computational mathematical modeling of the nonlinear vibration characteristics of AFG truncated conical nano pipe based on the nonlocal strain gradient theory", *Steel Compos. Struct.*, **42**(5), 599-619. https://doi.org/10.12989/scs.2022.42.5.599.

Zhang, L.H., Lai, S.K., Wang, C. and Yang, J. (2021), "DSC regularized Dirac-delta method for dynamic analysis of FG graphene platelet-reinforced porous beams on elastic foundation under a moving load", *Compos. Struct.*, **255**, 112865. https://doi.org/10.1016/j.compstruct.2020.112865.

Zhou, C., Zhang, Z., Zhang, J., Fang, Y. and Tahouneh, V. (2020), "Vibration analysis of FG porous rectangular plates reinforced by graphene platelets", *Steel Compos. Struct.*, **34**(2), 215-226, https://doi.org/10.12989/scs.2020.34.2.215.

Zhou, L. and Najjari, Y. (2022), "Analytical solution of buckling problem in plates reinforced by Graphene platelet based on third order shear deformation theory", *Steel Compos. Struct.*, **43**(6), 725-734. https://doi.org/10.12989/scs.2022.43.6.725.

Zhou, X., Wang, Y. and Zhang, W. (2021), "Vibration and flutter characteristics of GPL-reinforced functionally graded porous cylindrical panels subjected to supersonic flow", *Acta Astronaut.*, **183**, 89-100. https://doi.org/10.1016/j.actaastro.2021.03.003.

CC